Nanostructures

International Edition: DOI: 10.1002/anie.201500947
German Edition: DOI: 10.1002/ange.201500947

Platinum Multicubes Prepared by Ni^{2+}-Mediated Shape Evolution Exhibit High Electrocatalytic Activity for Oxygen Reduction**

Liang Ma, Chengming Wang, Bao Yu Xia, Keke Mao, Jiawei He, Xiaojun Wu, Yujie Xiong, and Xiong Wen (David) Lou**

Abstract: *Pt(100) facets are generally considered less active for the oxygen reduction reaction (ORR). Reported herein is a unique Pt-branched structure, a multicube, whose surface is mostly enclosed by {100} facets but contains high-index facets at the small junction area between the adjacent cubic components. The synthesis is accomplished by a Ni^{2+}-mediated facet evolution from high-index {311} to {100} facets on the frameworks of multipods. Despite the high {100} facet coverage, the Pt multicubes exhibit impressive ORR activity in terms of half-wave potential and current density nearly to the level of the most active Pt-based catalysts, while the durability of catalysts is well retained. The facet evolution creates a set of samples with tunable ratios of high-index to low-index facets. The results reveal that the excellent ORR performance of Pt multicubes is a combined result of active sites by high-index facets and low resistance by flat surface. It is anticipated that this work will offer a new approach to facet-controlled synthesis and ORR catalysts design.*

The oxygen reduction reaction (ORR) represents a highly important cathodic process in proton-exchange membrane fuel cells (PEMFC) and it may meet the increasing energy and environmental demands.[1–3] Like other catalytic systems, the ORR is one of the most structure-sensitive reactions in electrochemical energy conversion, and makes the surface facets of Pt electrocatalysts a versatile knob for tuning their energy conversion efficiencies.[4–8] Previous research on various Pt electrocatalysts has suggested that the half-wave potential ($E_{1/2}$) of ORR polarization on Pt low-index facets is in the order of $(100) \ll (111) < (110)$ in the perchloric acid system.[9,10] Nevertheless, the interlaced (111)-(100) Pt surface at the nanoscale is found to help enhance the ORR activity, most likely because of a synergetic effect between different facets.[11] It is proposed that molecular oxygen (O_2) is better adsorbed onto the (100) facets, followed by the diffusion of the adsorbed O_2 to the neighboring (111) facets where OH species are produced and easily released owing to their weak binding. Such a synergetic function enables high-index stepped facets such as (211), (331), and (311) to have higher ORR activity than the low-index facets.[9–11] For this reason, tremendous efforts have been made to construct high-index facets on Pt nanocrystals for ORR studies.[12–17]

Despite the common perception of superior ORR activities for Pt high-index facets relative to {100} facets, it remains an open question as to whether it is feasible to achieve high ORR performance on Pt nanocrystals having a large {100} surface coverage. Herein, we demonstrate the synthesis of a novel Pt-branched structure, multicube, whose surface is mostly enclosed by {100} facets but contains a small portion of high-index facets at the junction area between the adjacent cubic components. Such a unique structure exhibits strikingly high ORR performance in terms of activity ($E_{1/2}$ and current density) and durability, and nearly achieves the activity reported for Pt nanocrystals enriched with a stepped surface.[15]

Our synthesis involves a very interesting facet evolution with the assistance of Ni^{2+} cations as illustrated in Figure 1 a. The Ni^{2+} cation is selected as the foreign cation for inducing the facet evolution because Ni^{2+} possesses a d-electronic structure similar to that of Pt^{II}. It is well established that in the synthesis of Pt nanocrystals, $[PtCl_6]^{2-}$ should be firstly converted into a Pt^{II} species which is further reduced and nucleated on the Pt surface.[18] The comparable d-electronic structure of Ni^{2+} to Pt^{II} would reduce the probability of inducing effects other than surface-energy modification. In the synthesis, Pt-branched nanocrystals with high-index facets are firstly obtained in a simple reaction system at $t = 4$ h. Figures 1 b and c show transmission electron microscopy (TEM) and scanning TEM (STEM) images of the sample collected at $t = 4$ h. The images indicate that the branched nanocrystals have an average outer size of 20 nm, and have very round corners and a rough surface on each branch (named multipods). High-resolution TEM (HRTEM) images together with the fast Fourier transform (FFT) pattern in

[*] L. Ma,[+] Dr. C. Wang,[+] K. Mao, J. He, Prof. X. Wu, Prof. Y. Xiong
Hefei National Laboratory for Physical Sciences at the Microscale, Collaborative Innovation Center of Chemistry for Energy Materials, School of Chemistry and Materials Science, and CAS Key Laboratory of Materials for Energy Conversion, University of Science and Technology of China
Hefei, Anhui 230026 (P. R. China)
E-mail: yjxiong@ustc.edu.cn
Homepage: http://staff.ustc.edu.cn/~yjxiong/
Dr. B. Y. Xia,[+] Prof. X. W. Lou
School of Chemical and Biomedical Engineering
Nanyang Technological University
62 Nanyang Drive, Singapore 637459 (Singapore)
E-mail: xwlou@ntu.edu.sg
[+] These authors contributed equally to this work.

[**] This work was financially supported by the NSFC (No. 21101145), the Recruitment Program of Global Experts, the CAS Hundred Talent Program, the Anhui Provincial Natural Science Foundation (No. 1508085MB24), and the Fundamental Research Funds for the Central Universities (No. WK2060190025, WK2090050027, WK2310000035).

Supporting information for this article (materials synthesis, sample characterizations, electrochemical characterizations, and computational methods) is available on the WWW under http://dx.doi.org/10.1002/anie.201500947.

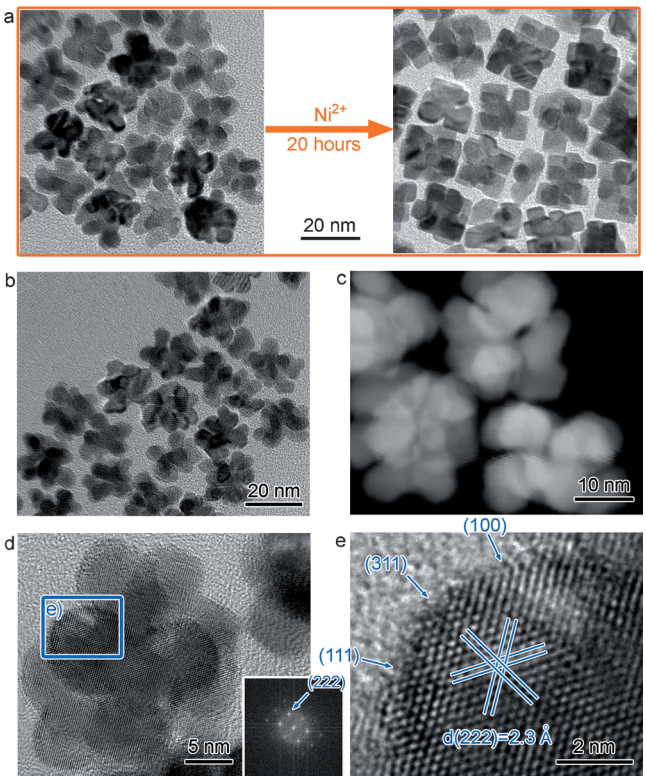

Figure 1. a) TEM images showing the morphological evolution from Pt multipods to multicubes in the presence of Ni^{2+} cations for 20 h. b) TEM, c) STEM, and d) HRTEM images of Pt multipods before the Ni^{2+}-mediated evolution. e) HRTEM image for the region marked by the blue box in (d). The inset of (d) shows the corresponding FFT pattern.

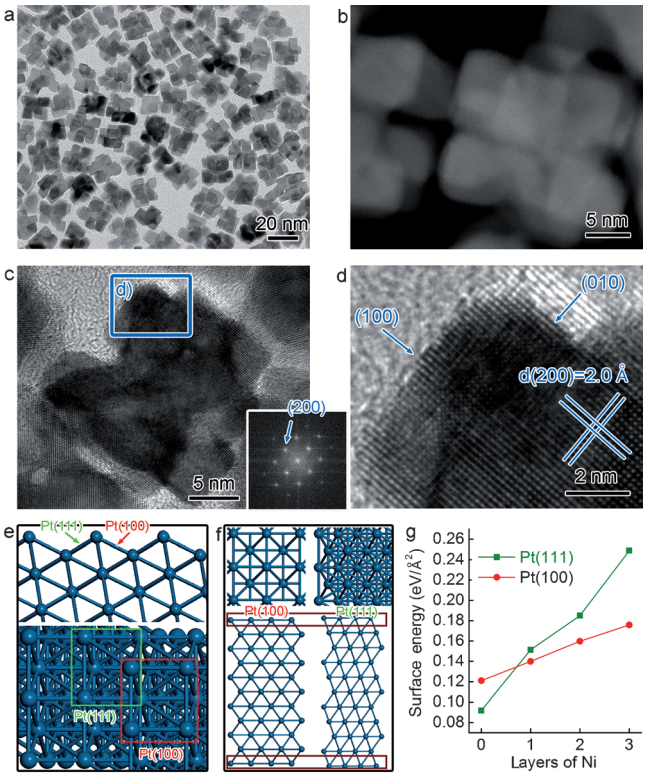

Figure 2. a) TEM, b) STEM, and c) HRTEM images of Pt multicubes after the Ni^{2+}-mediated evolution for 20 h. d) HRTEM image for the region marked by the blue box in (c). The inset of (c) shows the corresponding FFT pattern. e) Top- and side-views of the Pt(311) surface, consisting of a Pt(100) (in red box) and Pt(111) (in green box) surface. f) Top- and side-views of the Pt(111) and Pt(100) slabs. The atoms in brown boxes are the atoms in the outermost Pt layer and substituted by Ni in our calculations. g) Dependence of surface-formation energy on Ni coverage for Pt(111) and Pt(100).

Figure 1 d and e suggest that the surface is largely covered by {311}, {100}, and {111} facets.

Surprisingly, the multipods can evolve into a new type of branched structure by running the synthesis for another 20 h after $NiCl_2$ is added to the reaction system at $t = 4$ h. As shown in Figures 2 a and b, the resultant nanocrystals inherit branched structures from the multipods, but their branches appear to have sharp corners and exhibit a cubic shape. The HRTEM characterization (Figure 2 c and d) clearly shows that the surface is enclosed by {100} facets like nanocubes. Thus this new structure can be considered an assembly of multiple nanocubes sharing a common corner (named multicubes). It is clear that an evolution from high-index {311} facets to {100} facets occurs upon addition of the Ni^{2+} cations, for which the process has been clearly resolved by capturing the products at different reaction stages (see Figure S1 in the Supporting Information). The evolution gradually reduces the ratio of high-index to low-index facets, and produces a set of samples with tunable structures for investigating structure–property relationships in ORRs. Despite the structural evolution, the particle size (ca. 20 nm) remains similar throughout the process. Although the shape of the nanocrystals has been significantly altered with the addition of $NiCl_2$, they appear to be pure Pt with no Ni incorporated, as indicated by X-ray powder diffraction (XRD), energy-dispersive X-ray spectroscopy (EDS), and X-ray photoelectron spectroscopy (XPS), as well as by inductively coupled plasma mass spectrometry (ICP-MS; see Figures S2–S4 in the Supporting Information).

To elucidate the role of $NiCl_2$, we have performed two control experiments. First, one synthesis is conducted under the same experimental conditions except for the addition of $NiCl_2$. In the second synthesis, $NiCl_2$ is replaced with KCl while keeping other conditions unchanged. Interestingly, the nanocrystals do not transform into multicubes in both syntheses (see Figure S5 in the Supporting Information). Upon observing the importance of Ni^{2+} to facet evolution, it remains elusive as to why such guest ions can have significant effects on the development of Pt facets. Previously, it was reported that the addition of trace amounts of either Cu^{2+} or Ag^{+} can significantly alter the shapes and surface facets of noble-metal nanocrystals such as Pt, Ag, Au, and Pd, and an underpotential deposition (UPD) process is probably responsible for such a facet evolution.[19–22] However, it still remains elusive as to what roles the foreign cations play on the facet evolution.

To better uncover the mechanism, we employed first-principles to calculate the surface-formation energy of Pt, simulations which can reflect the relative stability of the Pt

surface. As shown in Figure 2e, a Pt(311) surface consists of Pt-(111) and Pt(100) steps. In the case of pristine Pt surface growth, the surface-formation energy for Pt-(111) is 0.092 eV Å^{-2}, which is lower by 0.029 eV Å^{-2} compared to a Pt(100) surface. Given the complex growth situation, this relatively small energy difference can be overwritten by many factors in practical experimental systems, thus resulting in the coexistence of Pt(111) and Pt(100) surfaces. Next, we gradually substitute Pt atoms in the first 1–3 layers with Ni atoms in our simulation model (Figure 2f) to assess the impact of Ni coverage on the surface-formation energy. Figure 2g shows the dependence of surface-formation energy on the number of Ni layers. Along with the implementation of Ni layers, both the Pt(111) and Pt(100) facets show gradually increased surface-formation energy, but the Pt(111) facet exhibits a stronger dependence. When the number of Ni layers reaches 3, the surface-formation energy of Pt(111) becomes 0.249 eV Å^{-2}, which is 0.073 eV Å^{-2} higher than that of Pt(100). As a result, it can be predicted that the coverage of Ni on a Pt(311) surface will make Pt(100) much more favorable compared to Pt(111). The fast growth on Pt(111) steps will cause the enlargement of Pt(100) at the expense of Pt(111), thus eventually leading to the exposure of (100) on surface.

We thus propose that the Ni^{2+} cations are quickly reduced to form a Ni UPD layer in the synthesis,[19–22] and can substantially alter the surface-formation energies of various facets to induce the shape evolution. As Ni is a metal with relatively high activity, the deposited Ni will inevitably undergo galvanic replacement with the $[PtCl_6]^{2-}$ precursor and Pt^{II} intermediate species during successive reactions.[23] As such, no elemental Ni has been detected in the final products, similar to the reported cases of UPD mechanism.[19–22] Apparently according to this mechanism, insufficient coverage of Ni is incapable of inducing the facet evolution, and as a result, the Pt structures exhibit a shape analogous to multipods when a low concentration of Ni^{2+} is used (see Figure S6 in the Supporting Information). However, excessive deposition of a Ni UPD layer would make the galvanic replacement occur unevenly on the surface, and is unfavorable for the formation of a well-defined multicube shape (see Figure S7 in the Supporting Information). It also turns out that this facet evolution process relies on the type of foreign metal cations used in the synthesis. For instance, the sample mainly maintains a multipod shape when $CuCl_2$ is used instead of $NiCl_2$ (see Figure S8 in the Supporting Information).

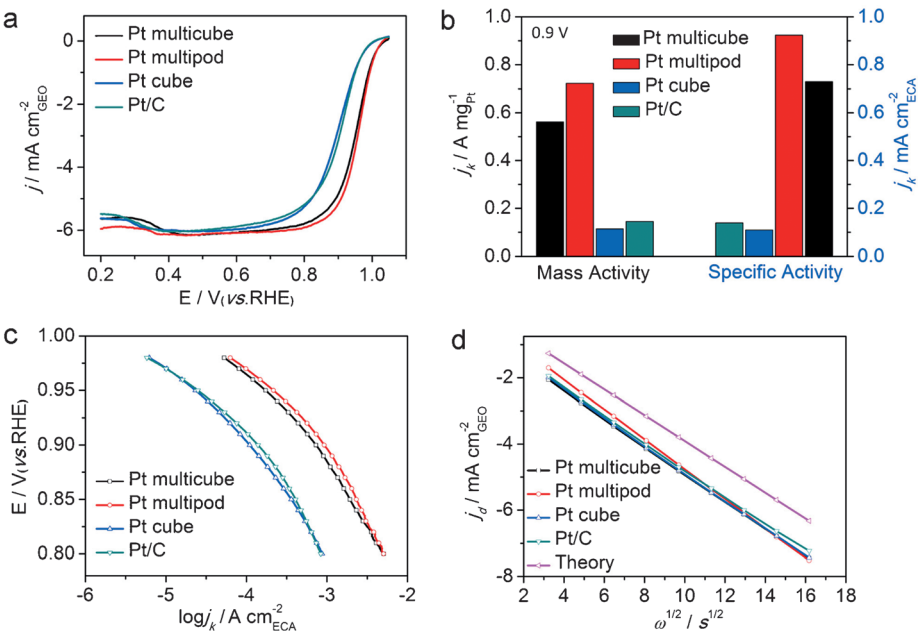

Figure 3. Comparison of electrochemical activities of Pt multicube and multipod samples with Pt/C and Pt cubes: a) ORR polarization curves in O_2-sataurated 0.1 M $HClO_4$ solution at room temperature. b) Mass activity and specific activity at 0.9 V versus RHE. c) Tafel plots. d) Koutecky-Levich plots. The potential scan rate is 20 mV s^{-1}, and the electrode rotation speed is 1600 rpm.

The as-formed Pt multicubes, made by this Ni^{2+}-mediated shape evolution, are ideal model particles for investigating whether high ORR activity can be achieved when Pt nanocatalysts are enclosed with high {100} surface coverage. We carried out ORR measurements in an O_2-saturated 0.1M $HClO_4$ solution on a glassy carbon (GC) rotating disk electrode (RDE) with a Pt loading of 45.86 μg cm^{-2} to evaluate the performance of our Pt nanocrystals in the present work. Figure 3a shows the ORR polarization curves for the Pt multicubes and multipods, benchmarked against the state-of-the-art Pt/C catalyst. The $E_{1/2}$ values of the Pt multicubes and multipods were determined to be 0.955 and 0.957 V, respectively, and are 50 and 52 mV higher than that of Pt/C catalysts (Table 1). Despite the relatively low Pt loading of these two samples, their high $E_{1/2}$ value appears comparable to the milestone value of 0.960 V for the porous Pt-Ni catalyst.[24] In particular, the Pt multicubes are bounded largely by {100} facets, in sharp contrast to the Pt multipods which have high-index facets, but still exhibit a high $E_{1/2}$ value.

Table 1: Half-wave potentials ($E_{1/2}$) of the ORR on GC RDEs prepared with four types of nanocatalysts.[a]

Catalysts	Pt/C	Pt cubes	Pt multipods	Pt multicubes
$E_{1/2\ \text{Initial}}$ (V vs. RHE)	0.905	0.899	0.957	0.955
$E_{1/2\ \text{After 10,000 cycles}}$ (V vs. RHE)	0.895	0.870	0.939	0.938

[a] The polarization curves were recorded in 0.1 M $HClO_4$ with continuous O_2 gas flow at a sweep rate of 20 mV s^{-1} and a rotation speed of 1600 rpm.

For comparison, we used Pt nanocubes enclosed by {100} facets (see Figure S9 in the Supporting Information) as a reference sample and the $E_{1/2}$ value turns out to be even 6 mV lower than that of Pt/C catalyst, thus verifying that Pt{100} facets have relatively low ORR activity as documented in the literature.[9,10] Thus the high activity of Pt multicubes should not be ascribed to their {100} surface facets.

The ORR activity can also be depicted by the mass activity and specific activity at 0.9 V (Figure 3b), which are obtained by normalizing the kinetic currents with Pt loading and electrochemical surface area (ECSA), respectively. The mass activity of the Pt multicube and multipod nanocatalysts reaches 0.562 and 0.722 A mg_{Pt}^{-1}, respectively, and are about 4.0 and 5.0 times higher than that of Pt/C catalyst. The specific activity of the Pt multicubes and multipods is 0.729 and 0.924 mA cm^{-2}, respectively, and 5.3- and 6.6-fold greater than that of Pt/C catalyst. In contrast, the mass and specific activities of Pt nanocubes (enclosed by {100} facets) are only 78.5 and 78.8%, respectively, of those of the Pt/C catalyst. The superior activities of Pt-branched structures to Pt nanocubes can be intuitively observed in the entire mixed kinetic-diffusion control region between 0.80 and 1.05 V (see Figure S10 in the Supporting Information), which are further confirmed by the Tafel plots for specific activity–potential relationships (Figure 3c). The Tafel slopes at a fixed potential are approximately identical, thus suggesting the same reaction mechanism over the majority of the potential range.[24,25] Furthermore, the Koutecky–Levich plots (Figure 3d) suggest that ORRs occurring on all the four different nanocatalysts undergoes a four-electron-transfer mechanism (see Figure S11 in the Supporting Information).[26]

The information of ORR activities gleaned above brings a question to our attention: why do the Pt multicubes exhibit comparable ORR activity to that of the multipods although they have such different surface facets? In other words, it is imperative to investigate the factors responsible for the superior ORR performance of the multicubes enclosed by Pt{100} facets. TEM images in Figure 2 provided valuable information about the shape and most surface of Pt multicubes. However, it remains challenging to resolve the exact structure in the junction area between the adjacent cubic components. We have thus opted to employ electrochemical characterizations which have been proven a valid tool to in situ determination of the surface structures of Pt nanoparticles.[27,28] The blank cyclic voltammograms (CVs) normalized by ECSA for all four Pt samples in Ar-purged 0.1 M $HClO_4$ are shown in Figure 4a–d. The blank CVs exhibit two potential regions: one between 0.05 and 0.4 V, which is attributed to the adsorption/desorption processes of underpotentially deposited hydrogen, and the other beyond about 0.6 V, thus corresponding to OH adlayers and oxide formation.[29,30] In general, the blank CVs can identify the presence of adsorption states of H to (110) and (100) step sites at about 0.13 and 0.27 V, respectively, and the superimposing broad current wave originated from the H adsorption at (111) sites.[27,28,31] Despite their very different morphologies, the CV of Pt multicubes (Figure 4a) turns out to exhibit analogous features to that of the Pt multipods (Figure 4b), in which (110), (111), and (100) step sites can be resolved. This finding suggests that the multicubes may possess a small portion of high-index facets composed of (111), (100), and (110) steps and terraces like those in the multipods.[27,32,33] Meanwhile, the CV of Pt multicubes also displays distinct (100) features similar to

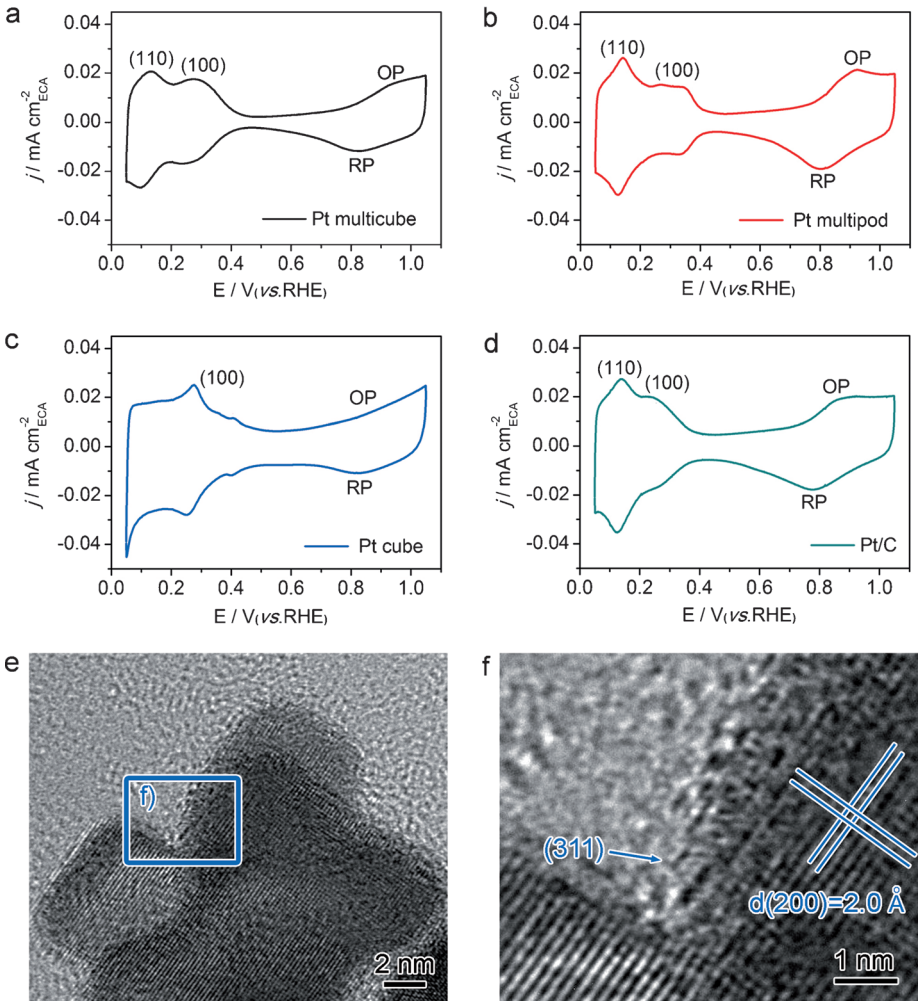

Figure 4. Blank CV curves recorded in Ar-saturated 0.1 M $HClO_4$ solution at a scan rate of 20 mV s^{-1}: a) Pt multicubes. b) Pt multipods. c) Pt cubes. d) Pt/C. e,f) HRTEM images of a Pt multicube with a focus on the junction area between the adjacent cubic components.

those for the {100}-enclosed Pt nanocubes (Figure 4c), because of the dominance of {100} facets on surface. Note that the CV profile obtained from the Pt/C catalyst with irregular morphologies (Figure 4d) appears similar to that reported for polycrystalline Pt electrodes.[34]

To further confirm the existence of high-index facets in the junction area, we attempted to collect HRTEM images (Figure 4e and f) by slightly tilting the sample. The images show that a small portion of high-index facets, such as {311}, exist in the junction area between the adjacent cubic components of a multicube. This observation combined with the CV measurements further proves the validity of our investigations above in accordance with previous reports.[27,28,31]

The oxidation potentials (OP) and reduction potentials (RP) for the four samples are also indicated in the blank CVs (Figure 4a–d). The Pt multicubes possess an OP value of about 0.93 V, which is higher than that for the Pt mutipods (ca. 0.92 V) and Pt/C catalyst (ca.0.86 V). In comparison, the Pt nanocubes do not show clear OP, thus implying relatively low oxidation resistance and stability.[15,29] In contrast, the onset potential from the ORR polarization curves (Figure 3a) clearly shows positive shift in the order: Pt cube < Pt/C < Pt multipod < Pt multicube. This finding suggests that our Pt multicubes have higher resistance to oxidation than the commercial Pt/C and Pt nanocubes.[15,29,30] The improved ORR performance stability has also been indicated by accelerated durability tests (i.e., see blank CVs in Figure S12, ECSA in Table S1, and ORR activities in Figures S13–S15 in the Supporting Information).

Upon recognizing the excellent ORR performance of Pt multicubes, another question would be: why does such a small portion of high-index facets enable high ORR activity? To address this question, we compared the electrochemical properties of Pt multipods and multicubes with that of their evolution intermediates. Both HRTEM images and blank CVs (see Figures S1 and S16 in the Supporting Information) reveal that the portion of high-index facets on the surface is gradually reduced with the evolution of multipods into multicubes. This decrease in high-index facet coverage should constantly reduce the ORR activity. However, a turning point between 4 and 12 hours during the shape evolution was observed for the ORR performance (see Figure S17 in the Supporting Information). Looking into the morphologies of samples, it can be recognized that the turning point is associated with the formation of a flat surface. Thus we speculate that the flat surface of Pt nanocrystals can promote their contact with electrodes and reduce contact resistance, and it has been further verified by electrochemical impedance spectroscopy (EIS; see Figure S18 in the Supporting Information). Thus the excellent ORR performance of Pt multicubes is a combined result of active sites on high-index facets and low resistance on the flat surface.

In summary, we have developed a unique Ni^{2+}-mediated facet-evolution approach to prepare Pt multicubes, which show excellent ORR activity and durability. The multicubes manifest comparable ORR performance to that of multipods with high-index facets, even though they are mostly enclosed by {100} facets, similar to the surface of cubes, with significantly lower ORR activity. One major finding in this work is that introduction of a small fraction of a highly active surface (i.e., the tiny junction area) together with the low contact resistance, enabled by a relatively flat surface, may lead to a big improvement on the catalytic performance of nanocrystals. We envision that the present work will provide new insights into rational tailoring of the surface of nanocatalysts.

Keywords: electrochemistry · nanostructures · oxygen · platinum · surface analysis

How to cite: *Angew. Chem. Int. Ed.* **2015**, *54*, 5666–5671
Angew. Chem. **2015**, *127*, 5758–5763

[1] G. Wu, K. L. More, C. M. Johnston, P. Zelenay, *Science* **2011**, *332*, 443.
[2] J. Greeley, I. E. L. Stephens, A. S. Bondarenko, T. P. Johansson, H. A. Hansen, T. F. Jaramillo, J. Rossmeisl, I. Chorkendorff, J. K. Nørskov, *Nat. Chem.* **2009**, *1*, 552.
[3] R. Bashyam, P. Zelenay, *Nature* **2006**, *443*, 63.
[4] H. You, S. Yang, B. Ding, H. Yang, *Chem. Soc. Rev.* **2013**, *42*, 2880.
[5] V. R. Stamenkovic, B. S. Mun, K. J. J. Mayrhofer, P. N. Ross, N. M. Markovic, *J. Am. Chem. Soc.* **2006**, *128*, 8813.
[6] Z. Chen, M. Waje, W. Li, Y. Yan, *Angew. Chem. Int. Ed.* **2007**, *46*, 4060; *Angew. Chem.* **2007**, *119*, 4138.
[7] J. Zhang, K. Sasaki, E. Sutter, R. R. Adzic, *Science* **2007**, *315*, 220.
[8] S. Guo, S. Zhang, S. Sun, *Angew. Chem. Int. Ed.* **2013**, *52*, 8526; *Angew. Chem.* **2013**, *125*, 8686.
[9] A. Kuzume, E. Herrero, J. M. Feliu, *J. Electroanal. Chem.* **2007**, *599*, 333.
[10] M. D. Maciá, J. M. Campina, E. Herrero, J. M. Feliu, *J. Electroanal. Chem.* **2004**, *564*, 141.
[11] V. Komanicky, A. Menzel, H. You, *J. Phys. Chem. B* **2005**, *109*, 23550.
[12] B. Lim, M. Jiang, P. H. C. Camargo, E. C. Cho, J. Tao, X. Lu, Y. Zhu, Y. Xia, *Science* **2009**, *324*, 1302.
[13] T. Yu, D. Y. Kim, H. Zhang, Y. Xia, *Angew. Chem. Int. Ed.* **2011**, *50*, 2773; *Angew. Chem.* **2011**, *123*, 2825.
[14] L. Ma, C. Wang, M. Gong, L. Liao, R. Long, J. Wang, D. Wu, W. Zhong, M. Kim, Y. Chen, Y. Xie, Y. Xiong, *ACS Nano* **2012**, *6*, 9797.
[15] C. Wang, L. Ma, L. Liao, S. Bai, R. Long, M. Zuo, Y. Xiong, *Sci. Rep.* **2013**, *3*, 2580.
[16] B. Y. Xia, H. B. Wu, X. Wang, X. W. Lou, *Angew. Chem. Int. Ed.* **2013**, *52*, 12337; *Angew. Chem.* **2013**, *125*, 12563.
[17] L. Ruan, E. Zhu, Y. Chen, Z. Lin, X. Huang, X. Duan, Y. Huang, *Angew. Chem. Int. Ed.* **2013**, *52*, 12577; *Angew. Chem.* **2013**, *125*, 12809.
[18] J. Chen, T. Herricks, Y. Xia, *Angew. Chem. Int. Ed.* **2005**, *44*, 2589; *Angew. Chem.* **2005**, *117*, 2645.
[19] H. Song, F. Kim, S. Connor, G. A. Somorjai, P. Yang, *J. Phys. Chem. B* **2005**, *109*, 188.
[20] M. L. Personick, M. R. Langille, J. Zhang, C. A. Mirkin, *Nano Lett.* **2011**, *11*, 3394.
[21] Y. Yu, Q. Zhang, J. Xie, J. Y. Lee, *Nat. Commun.* **2013**, *4*, 1454.
[22] A. R. Tao, P. Sinsermsuksakul, P. Yang, *Angew. Chem. Int. Ed.* **2006**, *45*, 4597; *Angew. Chem.* **2006**, *118*, 4713.
[23] R. C. Weast, *Handbook of Chemistry and Physics*, CRC Press, Boca Raton, FL, **1980**.
[24] J. Snyder, T. Fujita, M. W. Chen, J. Erlebacher, *Nat. Mater.* **2010**, *9*, 904.

[25] S. J. Clouser, J. C. Huang, E. Yeager, *J. Appl. Electrochem.* **1993**, *23*, 597.
[26] K. L. Hsueh, E. R. Gonzalez, S. Srinivasan, *Electrochim. Acta* **1983**, *28*, 691.
[27] J. Solla-Gullón, P. Rodríguez, E. Herrero, A. Aldaz, J. M. Feliu, *Phys. Chem. Chem. Phys.* **2008**, *10*, 1359.
[28] V. Grozovski, J. Solla-Gullón, V. Climent, E. Herrero, J. M. Feliu, *J. Phys. Chem. C* **2010**, *114*, 13802.
[29] V. R. Stamenkovic, B. S. Mun, M. Arenz, K. J. J. Mayrhofer, C. A. Lucas, G. F. Wang, P. N. Ross, N. M. Markovic, *Nat. Mater.* **2007**, *6*, 241.
[30] V. R. Stamenkovic, B. Fowler, B. S. Mun, G. F. Wang, P. N. Ross, C. A. Lucas, N. M. Markovic, *Science* **2007**, *315*, 493.
[31] J. Solla-Gullón, F. J. Vidal-Iglesias, A. Lòpez-Cudero, E. Garnier, J. M. Feliu, A. Aldaz, *Phys. Chem. Chem. Phys.* **2008**, *10*, 3689.
[32] J. Clavilier, K. Elachi, A. Rodes, *Chem. Phys.* **1990**, *141*, 1.
[33] A. Rodes, K. Elachi, M. A. Zamakhchari, J. Clavilier, *J. Electroanal. Chem.* **1990**, *284*, 245.
[34] J. Clavilier, J. P. Chauvineau, *J. Electroanal. Chem.* **1979**, *100*, 461.

Received: February 2, 2015
Published online: March 10, 2015

